

Differentiable Environment Primitives for Contact State Estimation

Kevin Haninger¹, Kangwagye Samuel², Filippo Rozzi³, Sehoon Oh², and Loris Roveda⁴

Abstract In contact-rich manipulation, the robot dynamics are coupled with an environment that has application-specific dynamic properties (stiffness, inertia) and geometry (contact normal). Knowledge of these environmental parameters can improve control and monitoring, but they are often unobserved and may vary, either online or between task instances. Observers, such as the extended Kalman filter, can be used to estimate these parameters, but such model-based techniques can require too much engineering work to scale up to complex environments, such as multi-point contact.

To accelerate environment modeling, we propose environment primitives: parameterized environment dynamics that can be connected in parallel and are expressed in an automatic differentiation framework. This simplifies offline gradient-based optimization to fit model parameters and linearization of the coupled dynamics for an observer. This method is implemented for stiffness contact models, allowing the fitting of contact geometry and stiffness offline or their online estimation by an extended Kalman filter. This method is applied to a collaborative robot, estimating external force, contact stiffness, and contact geometry from the motor position and current. The estimates of external force and stiffness are compared with a momentum observer and direct force measurements.

1 Introduction

Many contact-rich tasks – opening a door, screwing a lid onto a bottle, inserting a plug – require robustness over variation in task parameters such as contact normal, object inertia, or contact stiffness. Robot control can be improved when these parameters are known or estimated, *e.g.*, estimating a door’s inertia can improve manipulation [1], and estimating environment stiffness can improve impedance control [2]. Additionally, most contact-aware planning methods assume knowledge of contact geometry [3, 4]. However, estimating these parameters can often require too much engineering work, limiting the use of complex environment models in robotics.

What are common models for environment dynamics? Contact between the robot and environment couples them as seen in Fig. 1, changing the robot’s effective dynamics. Classically, contact is considered as a kinematic constraint [5], *i.e.*, perfectly stiff. These models are common in contact planning [6], and ongoing work is improving the computation of constrained dynamics [7] and the efficiency of multi-point contact [8]. Alternatively, if the robot, gripper, or environment has meaningful compliance, contact can be modeled as stiffness. Such stiffness contact models have been effective for force control [2, 9], model predictive control [1], control of contact impacts [10], and task monitoring [11].

The effective environment stiffness is application-specific, requiring data-based identification. This can be done online. When force and position are measured, adaptive control [12, 13] or recursive least squares [1, 9] can be used. When force/torque (F/T) measurements from a sensor are not available, the environment stiffness can be estimated from the robot motor position and motor torque [2, 14], but this approach requires a model of the coupled robot/environment dynamics.

Another contact parameter is the contact geometry, often expressed as the contact Jacobian or a signed distance function [3]. It is often assumed that the contact geometry is known, especially in locomotion [4], or where it can be extracted from CAD data [6]. However, in manipulation

*This work was supported by the National Research Foundation of Korea (NRF) grant funded by the Korea government (MSIT) (No. 5120201213805) and the European Union’s Horizon 2020 research and innovation programme under grant agreement No. 101058521 – CONVERGING.

¹Department of Automation, Fraunhofer IPK, Berlin, Germany kevin.haninger@ipk.fraunhofer.de

²Department of Robotics and Mechatronics Engineering, DGIST, Daegu, 42988, Korea [[ksamuel27](mailto:ksamuel27@dgist.ac.kr), [sehoon](mailto:sehoon@dgist.ac.kr)]

³Politecnico di Milano, Department of Mechanical Engineering, Milano, Italy filippo.rozzi@mail.polimi.it

⁴Istituto Dalle Molle di Studi sull’Intelligenza Artificiale (IDSIA), Scuola Universitaria Professionale della Svizzera Italiana (SUPSI), Università della Svizzera Italiana (USI) IDSIA-SUPSI, Lugano, Switzerland loris.roveda@idsia.ch

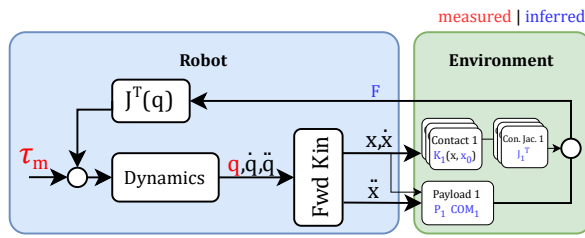


Figure 1: Robot interacting with the environment, with measured signals in red and unknown parameters in blue. The environment primitive is a parameterized function for the external force which depends on robot state. This paper implements and validates the contact stiffness and Jacobian with the environment primitive.

it may be desired to model contact without needing CAD, to enable interaction with natural world objects or simplify deployment. Contact geometry can also be estimated from data when F/T measurements are available [15] based on analytical models, which can also be done in collision detection to localize the collision [16]. Optimization-based approaches have also been proposed to identify contact geometry when F/T sensors are available [17].

Model-free methods can also be used in contact tasks. Classically, impedance control [18] is an interaction control method that does not require an environment model, but by itself does not provide a path forward to higher-level planning, monitoring, or control. The momentum observer [19, 20] is a method for estimating external force from motor current measurements, but these estimates must be post-processed to extract contact information. Data-driven methods have also been used to process contact information, such as a time-convolutional network trained in an end-to-end way [21], or using hand-defined higher-level features for classifying [22]. However, these methods do not produce models or controllers with understood generalizability, and direct learning of contact dynamics with current neural networks has been shown to have poor data-efficiency and limited generalizability [23].

A compromise solution to improve data-efficiency/generalizeability compared with data-driven approaches, and ease of deployment compared with model-based approaches, is to use parameterized, differentiable environment models. Automatic differentiation (AD) allows for the efficient computation of the derivative of complex functions composed of differentiable operations [24]. This allows efficient optimization of complex functions, which has been applied in robotics to learn dynamics [25], estimate friction parameters [26], and in contact model predictive control [6]. Today, the rigid-body dynamics and kinematics of robots are also available in AD frameworks [27].

This paper proposes differentiable environmental primitives, which are parameterized models of the environment force as a function of the robot state. The coupled robot/environment dynamics can be automatically gener-

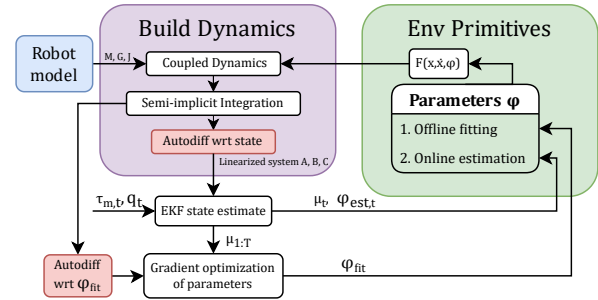


Figure 2: Total flow of the proposed process, where parameters can be fit offline or estimated online. The application of autodiff can be seen in red.

ated, and the parameters can be either fit offline by gradient-based optimization, or an extended Kalman Filter (EKF) used to estimate parameters online, as seen in Fig. 2. This process is simplified by AD, which supports gradient-based optimization for parameter fitting, generation of Jacobian matrices, and linearizing the dynamic/observation equations. By making the fitting and estimating of environment parameters easier, more complex models such as multi-contact and new environments become feasible.

Compared with typical contact models [6], this approach does not need contact geometry to be specified in advance. Compared with online stiffness estimation methods [1,2], the spatial contact normal is considered, and the contact point can be estimated. This paper is structured as follows: first, the continuous-time robot and environment models are introduced in Section 2, then the discrete system equations are derived in Section 3. Offline parameter fitting and online estimation are presented in Section 4. Experiments with a collaborative robot in Section 5 compare force and stiffness estimates with the momentum observer, and showing the feasibility of estimating contact geometry. All these estimation problems are derived from the same primitive, showing the flexibility of the approach.

1.1 Notation

A series $\bullet_{1:t} = [\bullet_1, \dots, \bullet_t]$, the normal distribution is $\mathcal{N}(\mu, \Sigma)$, the likelihood of a normal variable is $\mathcal{N}(x|\mu, \Sigma)$, and the next time step is $\bullet_+ = \bullet_{t+1}$.

2 Robot and Environment Primitives

This section introduces the models for robot dynamics, general environment primitives, and contact models.

2.1 Robot Dynamics

We assume the standard serial manipulator robot dynamics

$$M(q)\ddot{q} + C(q, \dot{q}) + B\dot{q} + G(q) = \tau_m + J^T(q)F \quad (1)$$

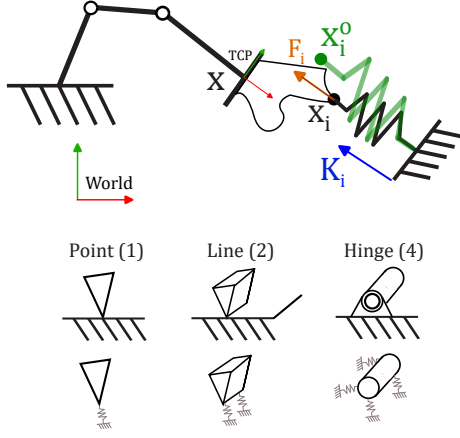


Figure 3: Stiffness contact model, where a contact point exerts only a normal force at a point on the robot. The geometry between the contact point and the end effector is assumed to be unknown but fixed. To model more complex kinematic constraints, multiple contact stiffnesses can be added in parallel.

and forward kinematics of

$$x = \ell(q), \quad \dot{x} = J(q)\dot{q}, \quad \ddot{x} = J(q)\ddot{q} + \dot{J}(q)\dot{q} \quad (2)$$

are available in an AD framework, with joint position $q \in \mathbb{R}^n$, inertia matrix $M(q)$, Coriolis terms $C(q, \dot{q})$, viscous damping B , gravitational torque $G(q)$, motor current τ_m , force at the tool-center point (TCP) F , TCP pose x and standard TCP Jacobian matrix $J(q)$. In the sequel, we simplify notation with the torque error

$$\tilde{\tau} = \tau_m - C(q, \dot{q}) - G(q). \quad (3)$$

2.2 Generic Environment Primitives

An environment primitive is a force element that acts on the robot, a function over both robot state and parameters as

$$F_i = F_i(x, \dot{x}, \phi_i), \quad (4)$$

with parameters $\phi_i \in \mathbb{R}^{p_i}$ and forces expressed in the TCP frame. When I primitives act on the robot in parallel, the total external force results in coupled robot environment dynamics of

$$M(q)\ddot{q} + B\dot{q} = \tilde{\tau} + \sum_{i=1}^I J^T(q)F_i(x, \dot{x}, \phi_i) \quad (5)$$

$$= \tilde{\tau} + \tau_e(q, \dot{q}, \phi), \quad (6)$$

where $\tau_e = \sum_i J^T F_i$ is the total environment force in joint space and ϕ the set of all primitive parameters ϕ_i .

2.3 Point Stiffness Contact Primitive

Consider a contact model as seen in Fig. 3, where the contact force F_i at the point of contact is expressed as

$$F_i = K_i^T (x_i^o - x_i), \quad (7)$$

where stiffness $K_i \in \mathbb{R}^3$ has a rest pose at $x_i^o \in \mathbb{R}^3$, and the contact point $x_i(q) \in \mathbb{R}^3$ has a fixed position in TCP frame. We can rewrite x_i as

$$x_i = T_{ee}^w \begin{bmatrix} x_i^{ee} \\ 1 \end{bmatrix}, \quad (8)$$

where T_{ee}^w is a homogeneous matrix transforming from the TCP to world frame, and $x_i^{ee} \in \mathbb{R}^3$ is x_i expressed in the TCP frame. The contact normal and stiffness are jointly described by the vector $K_i \in \mathbb{R}^3$, i.e., the contact normal is $n_i = K_i / \|K_i\|$, and the stiffness is $\|K_i\|$. For a single point stiffness, the joint torque induced is $\tau_e = J_i^T F_i$, where $J_i = \partial n_i^T x_i / \partial q$.

3 Discretized Linearized Dynamics

This section derives the discretized dynamics and linearizes them.

3.1 Integrator

As typical in contact models, we use semi-implicit integration which handles stiff differential equations better [5, 28]. For a time step of h , denoting the next time step of a variable \bullet_+ and dropping the argument of q ,

$$q_+ = q + h\dot{q}_+ \quad (9)$$

$$\begin{aligned} \dot{q}_+ &= \dot{q} + hM^{-1}(\tilde{\tau} + \tau_e - B\dot{q}_+) \\ &= (I + hM^{-1}B)^{-1}(\dot{q} + hM^{-1}(\tilde{\tau} + \tau_e)). \end{aligned} \quad (10)$$

We note that $(I + hM^{-1}B)^{-1} = I - h(M + hB)^{-1}B$ [29, (157)], and simplify the dynamics as

$$q_+ = q + h\dot{q} + h^2\delta \quad (11)$$

$$\dot{q}_+ = \dot{q} + h\delta \quad (12)$$

$$\delta = -(M + hB)^{-1}B\dot{q} + (I + hM^{-1}B)^{-1}M^{-1}(\tilde{\tau} + \tau_e),$$

where δ is the impulse caused by damping terms, torque error $\tilde{\tau}$ and contact torque τ_e . Note it simplifies to $\delta = M^{-1}(\tilde{\tau} + \tau_e)$ if $B = 0$. As τ_e depends on the contact primitive parameters ϕ , the dynamics can be written as

$$\begin{bmatrix} q_+ \\ \dot{q}_+ \end{bmatrix} = f \left(\begin{bmatrix} q \\ \dot{q} \end{bmatrix}, \tilde{\tau}, \phi \right). \quad (13)$$

3.2 Linearized Dynamics

For an EKF, the dynamics (13) must be linearized with respect to the state. When a parameter $\phi_{est} \in \mathbb{R}^e$ is to be estimated online, this results in a state

$$\xi = [q^T, \dot{q}^T, \phi_{est}^T]^T. \quad (14)$$

The system dynamics of (13) can then be linearized to find linear equations of

$$\begin{aligned}\xi_+ &= \begin{bmatrix} I & hI & h^2 \frac{\partial \delta}{\partial \phi_{est}} \\ h \frac{\partial \delta}{\partial q} & (I + hM^{-1}B)^{-1} & h \frac{\partial \delta}{\partial \phi_{est}} \\ 0 & 0 & I \end{bmatrix} \xi + b \\ &= A\xi + b + w,\end{aligned}\quad (15)$$

with process noise $w \sim \mathcal{N}(0, Q)$ and bias terms in b . In (15), the dependence of τ_e on q, \dot{q} is ignored to simplify the notation - these terms are be automatically calculated with the AD framework to give the complete linearized dynamics.

4 State and Parameter Estimation with Primitives

The parameters ϕ depend on the environment and task and may need to be fit offline, or estimated online. Parameters that are fit offline, as introduced in Section 4.1, are denoted ϕ_{fit} . The fit parameters update the primitives and are set to their optimized numerical values at runtime. Then, any parameters to be estimated online ϕ_{est} are estimated with the EKF as introduced in Sec. 4.2.

4.1 Offline Parameter Fitting

An advantage of the AD framework is that gradient-based optimization can be more easily implemented without needing to put the problem in a standard form such as least-squares because the derivative of objective functions and constraints over the optimization variables can be calculated by the AD framework. To fit contact model parameters, we apply a simplified expectation maximization approach [30] for the fitting of the parameters [31]. The expectation maximization approach makes iterative passes where i) the full state trajectory ξ_t is estimated with the Kalman filter as outlined in 4.2 to produce state mean and covariance $[\mu_{1:T}, \Sigma_{1:T}]$, then ii) the model parameters are optimized with $\mu_{1:T}$.

In the model parameter optimization step, the dynamic model is fit to minimize the least-squares prediction error as

$$\begin{aligned}\phi_{fit} &= \arg \min_{\phi} \sum_{t=1}^T \|\mu_{t+1} - f(\mu_t, \tau_{m,t}, \phi)\| \\ &\quad + 0.5\|x_{i,t} - x_i^o\| + \beta_{K_i}\|K_i\|_1 + \beta_{x_i}\|x_i\|,\end{aligned}\quad (16)$$

where β_{\bullet} is regularization ($\beta_{K_i} = 1e-9$, and $\beta_{x_i} = 5$), and $x_{i,t}$ is the contact position x_i at time t .

Note that this objective function is not the log-likelihood, as Σ_t^{-1} is not used - this is because the steady-state Kalman covariance dominates and Σ_t is almost constant. For computational load, the state is subsampled, choosing equally spaced pairs from the state trajectory, here, around 2000 points are used.

4.2 Online EKF

The observer estimates the complete state ξ , which includes robot state q, \dot{q} and parameters ϕ_{est} which are being estimated online. We assume a Gaussian distribution of the state and denote the posterior belief at time t as

$$p(\xi_t | q_{1:t}^m, \tau_{m,1:t}) = \mathcal{N}(\mu_t, \Sigma_t), \quad (17)$$

where q^m are measured joint positions, governed by

$$q^m = C\xi + v, \quad (18)$$

where $C = [I_n, 0_n, 0_p]$, $v \sim \mathcal{N}(0, R)$ is the measurement noise, assumed to be independent and identically distributed, I_n is an identity matrix of dimension n , and 0_n a square zero matrix of dimension n . An EKF is then implemented in joint space with belief space update of [32]

$$\begin{aligned}\bar{\Sigma} &= A\Sigma A^T + Q \\ L &= \bar{\Sigma} C^T (C\bar{\Sigma} C^T + R)^{-1}\end{aligned}\quad (19)$$

$$\mu_+ = Lq_+^m + (I - LC)f(\mu, \tau_m) \quad (20)$$

$$\Sigma_+ = (I - LC)\bar{\Sigma}, \quad (21)$$

where Σ is the error covariance matrix of the estimate, L is the Kalman gain, A is from (15), C is from (18), Q is the process noise covariance, and R is the measurement noise covariance.

4.3 Observability of Online Contact Estimation

When estimating contact parameters of (7) online, the question arises if K_i, x_i can be reliably estimated. We check the observability of this extended state via the observability matrix with A in (15) and C in (18), simplifying with damping $B = 0$ as

$$\begin{aligned}\mathcal{O} &= [C \quad CA \quad \dots \quad CA^{n-1}]^T \\ &= \begin{bmatrix} I & 0 & 0 \\ I & hI & h^2 \frac{\partial \delta}{\partial \phi_{est}} \\ I + h^2 \frac{\partial \delta}{\partial q} & 2hI & 2h^2 \frac{\partial \delta}{\partial \phi_{est}} \\ I + 3h^2 \frac{\partial \delta}{\partial q} & 3hI + h^3 \frac{\partial \delta}{\partial q} & 3h^2 \frac{\partial \delta}{\partial \phi_{est}} + h^4 \frac{\partial \delta}{\partial \phi_{est}} \frac{\partial \delta}{\partial q} \end{bmatrix}.\end{aligned}\quad (22)$$

To check the rank of the observability matrix \mathcal{O} , we first do row elimination, yielding

$$\mathcal{O} = \begin{bmatrix} I & 0 & 0 \\ 0 & hI & h^2 \frac{\partial \delta}{\partial \phi_{est}} \\ h^2 \frac{\partial \delta}{\partial q} & 0 & 0 \\ 3h^2 \frac{\partial \delta}{\partial q} & h^3 \frac{\partial \delta}{\partial q} & h^4 \frac{\partial \delta}{\partial \phi_{est}} \frac{\partial \delta}{\partial q} \end{bmatrix}. \quad (23)$$

We can then see that a necessary condition for full column rank is that the 2nd and 4th rows are linearly independent,

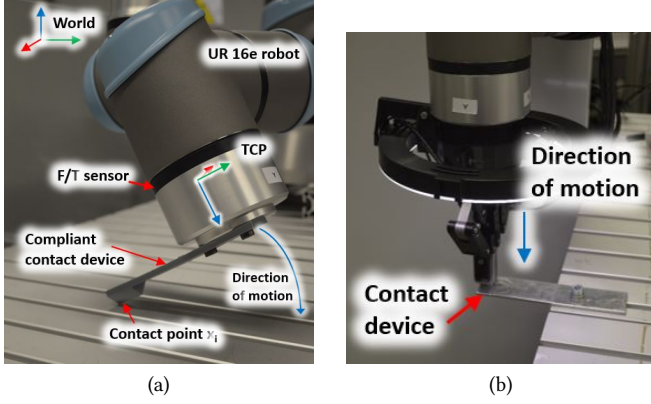


Figure 4: Experimental setup, (a) with a contact arm and single point of contact with the table, and (b) a vertical contact experiment.

i.e., their dot product is not zero. We find this dot product as

$$h^4 \frac{\partial \delta}{\partial q} + h^2 \left(\frac{\partial \delta}{\partial \phi_{est}} \right)^T h^4 \frac{\partial \delta}{\partial \phi_{est}} \frac{\partial \delta}{\partial q} \neq 0, \quad (24)$$

$$\left(I + h^2 \left(\frac{\partial \delta}{\partial \phi_{est}} \right)^T \frac{\partial \delta}{\partial \phi_{est}} \right) \frac{\partial \delta}{\partial q} \neq 0. \quad (25)$$

From the simplified expression in (25), we see that a necessary condition is that the partial derivative of the contact impulse with respect to robot joint $\partial \delta / \partial q \neq 0$, which is the case in stiffness models when M is non-singular and $\partial n_i^T x_i / \partial q \neq 0$.

5 Experimental Validation

This section describes the implementation and experimental validation of the proposed approach.

5.1 Hardware And Software Implementation

To validate the approach, a Universal Robots UR16e collaborative robot is outfitted with a gripper that has a variety of contact arms as seen in Fig. 4. An F/T sensor is integrated into the flange, which is used for admittance control and validation of estimated forces. The motor position and current are measured at 500 Hz. The gear-box ratios are found in the controller configuration files as [101, 101, 101, 54, 54, 54] and the motor torque constants as [0.119, 0.119, 0.098, 0.107, 0.107, 0.107].

The software is built on the AD framework CasADi [33]. For the fitting of parameters, IPOPT [34] is used. The robot dynamics and kinematics are built in Pinocchio [27] with CasADi support. The inertial model available from UR is used and modified to include the motor inertia on the diagonal elements. The code and experiment data are avail-

able at <https://gitlab.cc-asp.fraunhofer.de/hanikevi/full-state-estimator.git>.

The parameters used are a diagonal process noise with $1e-1$ on positions, $1e4$ on velocities, observation noise of $5e-2$, and viscous damping of $B = 0.2I$.

5.2 Momentum Observer and Stiffness Estimator

To benchmark, a momentum observer [19, 20] is used to estimate the TCP forces, finding the residual as

$$r_{t+1} = K_O (M_t \dot{q}_t - h(r_t - \tau_{e,t})), \quad (26)$$

where h is the time step, $M_t, \tau_{e,t}$ are from Section 3.1, and K_O the observer gain; $K_O = 20$ was used for each joint here. The residual was translated to TCP forces by

$$F_t^{mo} = (J^T)^+ r_t, \quad (27)$$

where \bullet^+ is the pseudoinverse and J the TCP Jacobian matrix.

The estimated force F_t^{mo} is used with the TCP position x_t to estimate the external stiffness K_t^{mo} as

$$K_t^{mo} = \frac{F_{t+W}^{mo} - F_t^{mo}}{\min(|x_{t+W} - x_t|, 5e-4)}, \quad (28)$$

where W is a smoothing window length and the denominator is modified to prevent division by zero.

5.3 Linear Contact Experiments

To compare the impact of the contact model on the estimate of robot state, three types of observers are compared. The observers are the EKF with the offline fit stiffness model, the EKF with online stiffness estimates, and the momentum observer.

In these experiments, the robot makes vertical contact with the contact stick shown in the inset of Fig. 4. The contact applies 105 N of force in the vertical direction by jogging the robot. The data is recorded and played back offline to give the same reference input to each observer.

5.3.1 Force estimate

The three observers are compared in their ability to estimate the TCP force, shown in Fig. 5, compared with the directly measured force. It can be seen that the momentum observer (blue) has high-frequency electrical noise, low-frequency error in the gravitational model, and discontinuities when the motion is stopped. Its major advantage is simplicity and independence from environment dynamics [20].

On the other hand, the EKF observers have reduced high-frequency noise characteristics and reduced low-frequency error to the measured force. An improvement is to be expected as they are including more information - and are

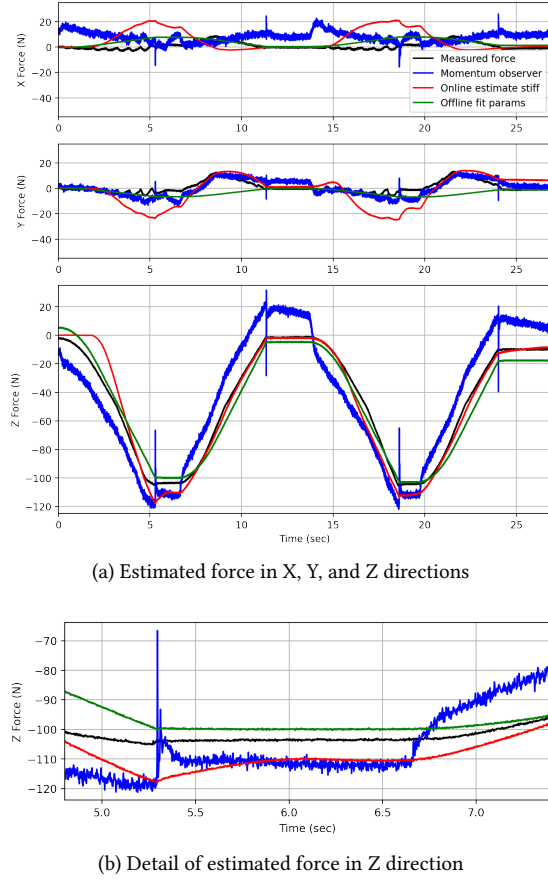


Figure 5: Comparison of estimated and measured force in the Z-contact task, forces shown in TCP coordinate frame

therefore environment-specific. The EKF with offline stiffness estimate (green) presents a smaller low-frequency error in the Z direction, and any discontinuities from the motor command are removed as this force is estimated over the robot state (joint position). The online estimate (red) also has a lower error in the Z direction, but a substantial lag in the estimate in the force (around 2.6 seconds from contact). This could not be addressed by tuning noise parameters or initial covariance, it is suspected that it may be influenced by off-diagonal elements in the covariance which are not initialized. The online EKF stiffness estimate performs comparably to the momentum observer in the X/Y direction.

5.3.2 Stiffness estimate

The observers are then compared in their ability to estimate the stiffness online, shown in Fig. 6. Here, the offline estimates provided by the method in Sec. 4.1 (green, 28.3 N/mm) are also compared with the least-squares fit of stiffness from the F/T sensor measurements and TCP pose (black, 25.8 N/mm).

It can be seen in Fig. 6(a) that the offline estimate of the environment stiffness is a reasonable approximation of the

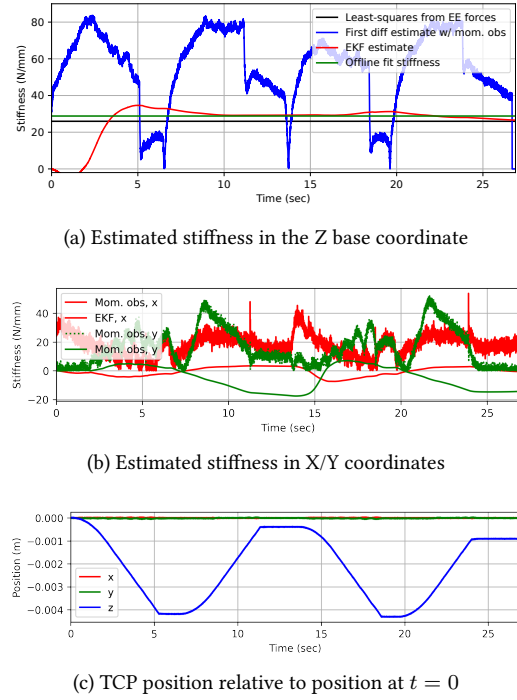


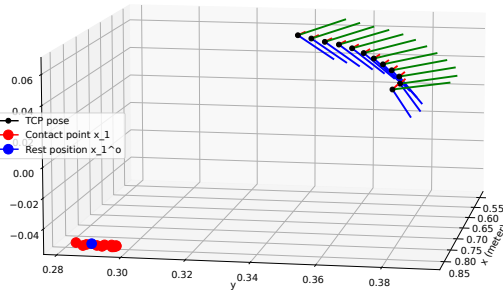
Figure 6: Vertical contact experiments with estimated stiffness (a), (b), and TCP position (c)

directly estimated stiffness, without needing the use of an F/T sensor. Some errors may be attributed to the stiffness being fit to reduce all dynamic errors, *i.e.*, it may include some gravitational errors. On the other hand, the online estimate of stiffness has more variation, taking approximately 2.6 seconds to rise to a reasonable value, and the magnitude varies as the direction of motion varies. The momentum observer estimate of stiffness is found with a moving-average window of $W = 50$ time steps or 0.01 seconds but remains noisy. It also has a much higher degree of variation during the task, also having large jumps when the residual of the momentum observer jumps due to the discontinuity in motor current.

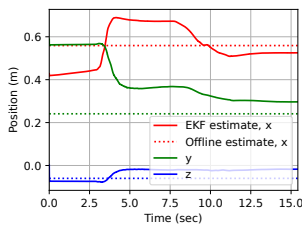
In the X and Y directions, the EKF estimates a much lower stiffness, whereas the momentum observer-based approach has higher average estimates of stiffness. This direction has much less motion, as can be seen in Fig. 6(c).

5.4 Rotation about a Single Point Contact

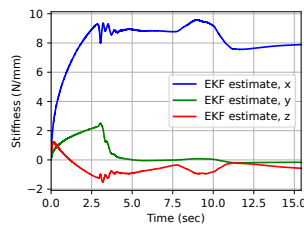
A single point contact is made with the contact arm as seen in Fig. 4(a), where the robot is then driven in the positive Z direction of the TCP by a desired force given to an admittance controller of 30 N. The point stays constant in these experiments as the friction was not exceeded, providing a single point of contact as the robot arcs around this point. The robot TCP and estimated contact parameters can be seen in Fig. 7(a), where contact stiffness K_1 , contact point x_1 and rest position x_1^o are fit offline by (16). The con-



(a) Motion of TCP (top right), rest position x_1^o , and estimated contact point x_1



(b) Online estimate of contact point x_1 in world coordinates



(c) Online estimate of stiffness K_1 in world coordinates

Figure 7: Single point rotation experiments, showing offline (a), and online estimates (b), (c).

tact point x_1 is fit to $x_1^{ee} = [0.023, -0.102, 0.051]$ (contact point relative to TCP), and hand measured at roughly $x_1^{ee} = [-0.020, -0.125, 0.020]$, indicating an error on the order of 2 – 4 cm per degree of freedom. The position of x_1 in world coordinates is plotted in Fig. 7 at each step with a red dot and has a variance of about 2 cm, also indicating a reasonable fit.

The the contact location x_1 is then estimated online, from initial point $x_1^{ee} = [0.2, 0.2, 0.2]$ with initial diagonal covariance $[1e9, 1e9, 1e9]$ and process noise $[10, 10, 10]$. The online estimate, in solid lines, is expressed in base coordinates and compared with the offline fit rest position in dotted lines - these should converge when no displacement occurs. The x and y estimates converge within 3 seconds to within 5 cm of the rest position.

The stiffness is then estimated online, using the offline fit x_1 and x_1^o , initial value $K_1 = [1, 1, 1]$, initial covariance $[1e13, 1e13, 1e13]$ and process noise $[1e10, 1e10, 1e10]$. The results can be seen in Fig. 7(c), where the estimated stiffness is shown in base coordinates. The Z-axis dominates, which is the primary direction of displacement in the task. However, the Z estimate has much more variation than seen in the vertical contact experiment.

6 Conclusion

This paper demonstrated a flexible approach for defining parameterized contact models in an AD framework, which supports offline fitting and online estimation in a unified framework. This methodology was verified in the estimation of translational stiffness in a one-point contact from motor current and position measurements. The approach was shown to have a delay in the online estimation of stiffness, but fewer problems when motion is limited compared with a first-difference estimate of stiffness. Using the approach to estimate external force has less noise compared to a momentum observer, and reduced low-frequency error, but requires additional implementation work. The estimate of contact point offline and online had worst-case error on the order of 2 and 7 cm, respectively, showing limited accuracy which could be attributed to the difficulty of estimating from joint motor position and current measurements. However, all these estimation problems can be addressed with a single computational model, demonstrating the flexibility of the framework.

References

- [1] M. V. Minniti, R. Grandia, K. F  h, F. Farshidian, and M. Hutter, “Model Predictive Robot-Environment Interaction Control for Mobile Manipulation Tasks,” *arXiv:2106.04202 [cs]*, Jun. 2021.
- [2] L. Roveda and D. Piga, “Sensorless environment stiffness and interaction force estimation for impedance control tuning in robotized interaction tasks,” *Autonomous Robots*, vol. 45, no. 3, pp. 371–388, 2021.
- [3] R. Tedrake, “Underactuated Robotics: Algorithms for Walking, Running, Swimming, Flying, and Manipulation (Course Notes for MIT 6.832),” *Downloaded on October 2020 from <http://underactuated.mit.edu>*, 2020.
- [4] J. Carius, R. Ranftl, V. Koltun, and M. Hutter, “Trajectory optimization with implicit hard contacts,” *IEEE Robotics and Automation Letters*, vol. 3, no. 4, pp. 3316–3323, 2018.
- [5] D. E. Stewart, “Rigid-Body Dynamics with Friction and Impact,” *SIAM Rev.*, vol. 42, no. 1, pp. 3–39, Jan. 2000.
- [6] C. Mastalli, R. Budhiraja, W. Merkt, G. Saurel, B. Hamdoun, M. Naveau, J. Carpentier, L. Righetti, S. Vijayakumar, and N. Mansard, “Crocodlyl: An Efficient and Versatile Framework for Multi-Contact Optimal Control,” in *2020 IEEE International Conference on Robotics and Automation (ICRA)*, May 2020, pp. 2536–2542.
- [7] J. Carpentier, R. Budhiraja, and N. Mansard, “Proximal and Sparse Resolution of Constrained Dynamic Equations,” in *Robotics: Science and Systems XVII*. Robotics: Science and Systems Foundation, Jul. 2021.

- [8] A. Aydinoglu and M. Posa, “Real-Time Multi-Contact Model Predictive Control via ADMM,” *arXiv:2109.07076 [cs]*, Mar. 2022.
- [9] R. Rossi, L. Fossali, A. Novazzi, L. Bascetta, and P. Rocco, “Implicit force control for an industrial robot based on stiffness estimation and compensation during motion,” in *Robotics and Automation (ICRA), 2016 IEEE International Conference On*. IEEE, 2016, pp. 1138–1145.
- [10] Y. Wang, N. Dehio, and A. Kheddar, “On Inverse Inertia Matrix and Contact-Force Model for Robotic Manipulators at Normal Impacts,” *IEEE Robot. Autom. Lett.*, vol. 7, no. 2, pp. 3648–3655, Apr. 2022.
- [11] K. Haninger and D. Surdilovic, “Multimodal Environment Dynamics for Interactive Robots: Towards Fault Detection and Task Representation,” in *Proc. IEEE/RSJ Intl Conf on Intelligent Robots and Systems (IROS)*, 2018, pp. 6932–6937.
- [12] N. Diolaiti, C. Melchiorri, and S. Stramigioli, “Contact impedance estimation for robotic systems,” *IEEE Transactions on Robotics*, vol. 21, no. 5, pp. 925–935, 2005.
- [13] M. Parigi Polverini, S. Formentin, L. Merzagora, and P. Rocco, “Mixed Data-Driven and Model-Based Robot Implicit Force Control: A Hierarchical Approach,” *IEEE Transactions on Control Systems Technology*, vol. 28, no. 4, pp. 1258–1271, Jul. 2020.
- [14] L. Roveda, D. Riva, G. Bucca, and D. Piga, “Sensorless Optimal Switching Impact/Force Controller,” *IEEE Access*, vol. 9, pp. 158 167–158 184, 2021.
- [15] D. Popov, A. Klimchik, and N. Mavridis, “Collision detection, localization classification for industrial robots with joint torque sensors,” in *2017 26th IEEE International Symposium on Robot and Human Interactive Communication (RO-MAN)*, Aug. 2017, pp. 838–843.
- [16] S. Haddadin, A. De Luca, and A. Albu-Schäffer, “Robot Collisions: A Survey on Detection, Isolation, and Identification,” *IEEE Transactions on Robotics*, vol. 33, no. 6, pp. 1292–1312, Dec. 2017.
- [17] S. Koley and E. Todorov, “Physically consistent state estimation and system identification for contacts,” in *2015 IEEE-RAS 15th International Conference on Humanoid Robots (Humanoids)*, Nov. 2015, pp. 1036–1043.
- [18] N. Hogan, “Impedance control: An approach to manipulation,” in *American Control Conference, 1984*. IEEE, 1984, pp. 304–313.
- [19] A. De Luca and R. Mattone, “Sensorless robot collision detection and hybrid force/motion control,” in *Robotics and Automation, 2005. ICRA 2005. Proceedings of the 2005 IEEE International Conference On*. IEEE, 2005, pp. 999–1004.
- [20] G. Garofalo, N. Mansfeld, J. Jankowski, and C. Ott, “Sliding mode momentum observers for estimation of external torques and joint acceleration,” in *2019 International Conference on Robotics and Automation (ICRA)*. IEEE, 2019, pp. 6117–6123.
- [21] D. Lee, K. Turitsyn, and J.-J. Slotine, “Robust Model Predictive Control for Nonlinear Systems Using Convex Restriction,” *arXiv:2003.00345 [math]*, Apr. 2021.
- [22] T. Migimatsu, W. Lian, J. Bohg, and S. Schaal, “Symbolic State Estimation with Predicates for Contact-Rich Manipulation Tasks,” Mar. 2022.
- [23] M. Parmar, M. Halm, and M. Posa, “Fundamental Challenges in Deep Learning for Stiff Contact Dynamics,” in *2021 IEEE/RSJ International Conference on Intelligent Robots and Systems (IROS)*, Sep. 2021, pp. 5181–5188.
- [24] A. G. Baydin, B. A. Pearlmutter, A. A. Radul, and J. M. Siskind, “Automatic differentiation in machine learning: A survey,” *Journal of Machine Learning Research*, vol. 18, pp. 1–43, 2018.
- [25] K. A. Smith, K. R. Allen, and J. B. Tenenbaum, “End-to-end differentiable physics for learning and control,” in *Advances in Neural Information Processing Systems*. Curran Associates Inc, 2018.
- [26] Q. Le Lidec, I. Kalevtykh, I. Laptev, C. Schmid, and J. Carpentier, “Differentiable Simulation for Physical System Identification,” *IEEE Robot. Autom. Lett.*, vol. 6, no. 2, pp. 3413–3420, Apr. 2021.
- [27] J. Carpentier, G. Saurel, G. Buondonno, J. Mirabel, F. Lamiroux, O. Stasse, and N. Mansard, “The Pinocchio C++ library: A fast and flexible implementation of rigid body dynamics algorithms and their analytical derivatives,” in *2019 IEEE/SICE International Symposium on System Integration (SII)*. IEEE, 2019, pp. 614–619.
- [28] K. Haninger, M. Radke, A. Vick, and J. Kruger, “Towards High-Payload Admittance Control for Manual Guidance with Environmental Contact,” *IEEE Robotics and Automation Letters*, 2022.
- [29] M. R. Pedersen, L. Nalpantidis, R. S. Andersen, C. Schou, S. Bøgh, V. Krüger, and O. Madsen, “Robot skills for manufacturing: From concept to industrial deployment,” *Robotics and Computer-Integrated Manufacturing*, vol. 37, pp. 282–291, 2016.
- [30] A. P. Dempster, N. M. Laird, and D. B. Rubin, “Maximum likelihood from incomplete data via the EM algorithm,” *Journal of the Royal Statistical Society: Series B (Methodological)*, vol. 39, no. 1, pp. 1–22, 1977.

- [31] J. Durbin and S. J. Koopman, *Time Series Analysis by State Space Methods*. OUP Oxford, 2012, vol. 38.
- [32] S. Thrun, “Probabilistic robotics,” *Communications of the ACM*, vol. 45, no. 3, pp. 52–57, 2002.
- [33] J. A. Andersson, J. Gillis, G. Horn, J. B. Rawlings, and M. Diehl, “CasADi: A software framework for nonlinear optimization and optimal control,” *Mathematical Programming Computation*, vol. 11, no. 1, pp. 1–36, 2019.
- [34] A. Wächter and L. T. Biegler, “On the implementation of an interior-point filter line-search algorithm for large-scale nonlinear programming,” *Mathematical programming*, vol. 106, no. 1, pp. 25–57, 2006.